ECS Journal of Solid State Science and Technology, **7** (11) P647-P650 (2018)
2162-8769/2018/7(11)/P647/4/$37.00 © The Electrochemical Society

Phase Change Behavior of $Sn_{20}Sb_{80}$/Si Nano-Composite Multilayer Thin Films

Xuan Guo,[1] Yifeng Hu,[1,2,3,z] Qingqian Chou,[4] Tianshu Lai,[4,z] Rui Zhang,[1] and Xiaoqin Zhu[1]

[1] *School of Mathematics and Physics, Jiangsu University of Technology, Changzhou 213000, People's Republic of China*
[2] *State Key Laboratory of Silicon Films, Zhejiang University, Hangzhou 310027, People's Republic of China*
[3] *Key Laboratory of Microelectronic Devices & Integrated Technology, Institute of Microelectronics, Chinese Academy of Sciences, Beijing 100029, People's Republic of China*
[4] *State-Key Laboratory of Optoelectronic Films and Technology, School of Physics, Sun Yat-Sen University, Guangzhou 510275, People's Republic of China*

Nano-composite multilayer $Sn_{20}Sb_{80}$/Si thin films were studied by thermal, electrical and optical methods. Compared with $Sn_{20}Sb_{80}$, $Sn_{20}Sb_{80}$/Si film was proved to be a more promising candidate for phase change memory device applications because of its higher crystallization temperature (246°C) and larger crystallization activation energy (2.6 eV). The bandgap was broadened with the increase of Si layer thickness. The crystallization of $Sn_{20}Sb_{80}$ was restrained after the adding of more Si film layers confirmed by X-ray diffraction patterns. A smoother surface was obtained with the root-mean-square surface roughness of 0.753 nm for $[Sn_{20}Sb_{80}(3nm)/Si(7nm)]_5$ thin film. The measurement using the picosecond laser technique showed that $[Sn_{20}Sb_{80}(3nm)/Si(7nm)]_5$ thin film could achieve the crystalline-to-amorphous phase transform within 2.8 ns irradiated by the laser pulse.
 [DOI: 10.1149/2.0131811jss]

Manuscript submitted August 13, 2018; revised manuscript received September 24, 2018. Published October 31, 2018.

With the rapid development of various mobile storage technologies in recent years, the demand for non-volatile memory is continuously increasing. Phase change memory (PCM), as a new type of semiconductor memory, has the advantages of multistage storage, ultrafast speed, radiation hardened, and compatibility with existing integrated circuit technology. The switching between the crystalline state (low resistance) and the amorphous state (high resistance) for the phase change film is the basic principle. The writing and erasing of information can be realized by the different electrical pulses. The crystallization process of the phase-change film by applying a low and wide electrical pulse is defined as the SET operation. The RESET one is to melt the phase-change film and cool it off quickly to form the amorphous state with a high and short pulse. The readout of information is achieved by applying a lower reading pulse to measure the change in the resistance of the device unit.

The chalcogenide is the storage medium of PCM. $Ge_2Sb_2Te_5$ (GST) is currently recognized as a relatively suitable storage material for PCM application in the industry because of its widely using in DVD. However, its crystallization temperature is only 165°C. Accordingly, the data can only be maintained at 85°C for 10 years, which cannot meet the requirements in archival storage.[1] The properties of phase-change films can be improved effectively by multi-layer composite with other films. A lower thermal conductivity of multilayer film is the superiority over monolayer-layer one, because it can effectively reduce the operating power consumption in PCM devices.[2] Nowadays, Sb-rich binary phase change films are getting more and more attention, such as Sn-Sb,[3] Al-Sb,[4] C-Sb[5] and Zn-Sb.[6] An ultrafast phase change rate is the enormous advantage. However, there are still some problems before their mass usage in PCM, such as frail thermal stability and poor data retention. In references, Ga_3Sb_7 and SiO_2 have been used to composite with $Sn_{20}Sb_{80}$ to improve its phase change property. Except for better thermal stability, $Sn_{20}Sb_{80}/Ga_3Sb_7$ as well as $Sn_{20}Sb_{80}/SiO_2$ multilayer thin films showed fast phase switching speed.[7,8] In addition, Si has shown good effect in Sb_2Se/Si multilayer thin film, including increasing the crystallization resistance and phase change temperature.[9] In this work, Si had been chosen as alternating layer to composite with $Sn_{20}Sb_{80}$ to form Chalcogenide Super Lattice (CSL). The effect of Si layers on $Sn_{20}Sb_{80}$ was investigated in details.

Experimental

At room temperature, $Sn_{20}Sb_{80}$ and Si target were used to prepare $Sn_{20}Sb_{80}$/Si multilayer thin films by means of magnetron sputtering. The purity of both targets was 99.999%. The substrate of the deposited film was SiO_2/Si (100) substrate. Before the substrate was used, the ultrasonic cleaning of acetone, ethanol and deionized water were carried out successively to remove dust, organic and inorganic impurities on the surface of the substrate. The temperature of the heating platform was regulated by the TP94 temperature control system (Linkam Scientific Instruments Ltd, UK), and the temperature was controlled by liquid nitrogen through the lnp94/2 cooling system. The vacuum degree of sputtering background was better than 1×10^{-4} pa. And the sputtering pressure, flow rate of high purity argon gas (99.999%) and sputtering power were set to 0.3 Pa, 30 SCCM (SCCM is standard ml/min) and 20 W respectively. In order to guarantee the room temperature of the substrate, the cooling water was used for circulating cooling during sputtering. By controlling the total thickness of the composite film and adjusting the thickness ratio of $Sn_{20}Sb_{80}$ to Si monolayer film, $Sn_{20}Sb_{80}$/Si nano-composite multilayer thin films with same periodicity were prepared.

The crystallization temperature of the thin films could be obtained by measuring the change of the resistance of the sample during the heating process through the in-situ resistance-temperature (*R-T*) test system. By studying the isothermal crystallization process at different temperatures, the crystal activation energy (E_c) and thermal stability could be evaluated.[10] In order to prevent the oxidation and volatilization of the film during heating, high purity Ar gas was led into the test chamber for protection. The transmittance spectrum of the film was measured in the wavelength range from 900 to 2500 nm by using a UV-visible-NIR spectrophotometer, and the optical bandgap was obtained by using the Tauc formula. X-ray powder polycrystalline diffractometer (XRD) using Cu Kα radiation in the 2θ range from 20° to 60° with a scanning step of 0.01° was used to characterize the crystalline phase structure before and after the crystallization. The surface morphology of the film was observed by atomic force microscope (AFM, FM-Nanoview 1000). The phase change rate of the composite film was evaluated by the laser picosecond pump-probe test system, in which the duration and wavelength of the light irradiated on the film were 30 ps and 532 nm, respectively.

Results and Discussion

In order to study the transition from amorphous to crystalline state, the temperature-dependent resistance change is measured for $Sn_{20}Sb_{80}$

[z]E-mail: hyf@jsut.edu.cn; stslts@mail.sysu.edu.cn

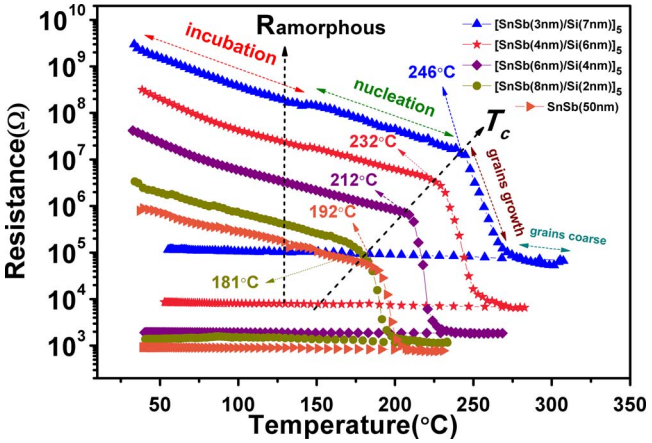

Figure 1. Resistance as a function of temperature for $Sn_{20}Sb_{80}$/Si multilayer composite thin films with different thickness ratio at a heating rate of 30°C/min.

monolayer-layer and $Sn_{20}Sb_{80}$/Si composite multilayer films. The films show high resistance at the initial stage, as shown in Fig. 1, indicating the amorphous state. In addition, the amorphous resistance of $Sn_{20}Sb_{80}$/Si films also increases with increasing thickness of Si, which is believed to be associated with the high resistivity of Si and the interfacial effect.[11] At the beginning, the resistance of all the films remains almost constant. As the heating time increases, the resistance of the films begins to decline slowly. When the incubation stage is completed, the film resistance begins to decrease at a fast speed, which is called the nucleation stage.[12] The temperature at which the resistance starts to decrease suddenly is defined as the crystallization temperature T_c of the films, and the derivative of the resistance relative to temperature (dR/dT) reaches a minimum.[13] The meaning of the inflection point is the transformation from nucleation stage to grain growth stage. As is seen in Fig. 1, the T_c of $Sn_{20}Sb_{80}$, $[Sn_{20}Sb_{80}(8nm)/Si(2nm)]_5$, $[Sn_{20}Sb_{80}(6nm)/Si(4nm)]_5$, $[Sn_{20}Sb_{80}(4nm)/Si(6nm)]_5$ and $[Sn_{20}Sb_{80}(3nm)/Si(7nm)]_5$ are 192, 181, 212, 232, and 246°C, respectively. In general, the thermal stability of phase change film has positive correlation with T_c. That is, as the thickness of the Si layer increases, the thermal stability of the $Sn_{20}Sb_{80}$/Si films improves as a whole. After T_c, the resistance has a rapidly decreasing process corresponding to grains growth stage and then remains at a lower and stable value. This means that the films have finished the crystallization, reaching grains coarse stage and forming a crystalline state of low resistivity.[14] It is noteworthy that the resistance is almost unchanged after subsequent cooling operations, indicating that the films remain at crystalline state in this process. What's more, the crystal resistance of the phase change thin films increases with the increasing of Si layer thickness. In the joule heating effect of the current pulse, a higher crystalline resistance helps to increase the efficiency of heating, thereby reducing the power consumption during the RESET operation.

The data reliability of phase change film can be further evaluated by performing isothermal crystallization testing. Figs. 2a and 2b are the curves of normalized resistance of the $[Sn_{20}Sb_{80}(6nm)/Si(4nm)]_5$ and $[Sn_{20}Sb_{80}(4nm)/Si(6nm)]_5$ thin films with annealing time. The lower the isothermal temperature, the longer the incubation period required.[15] The failure time is defined as the time when the resistance reduces to 50% of the initial value.[16] In Fig. 2a, the failure time of $[Sn_{20}Sb_{80}(6nm)/Si(4nm)]_5$ film at 185, 180 and 175°C are 73, 237 and 1080 s, respectively. Similarly, the failure time of $[Sn_{20}Sb_{80}(4nm)/Si(6nm)]_5$ composite films for 195, 190 and 185°C are 145, 731 and 1981 s, respectively.

According to the same test method, we also measured the failure time of other films. The failure time and isothermal temperature of different thin films were linearly simulated, and Fig. 2c was obtained.

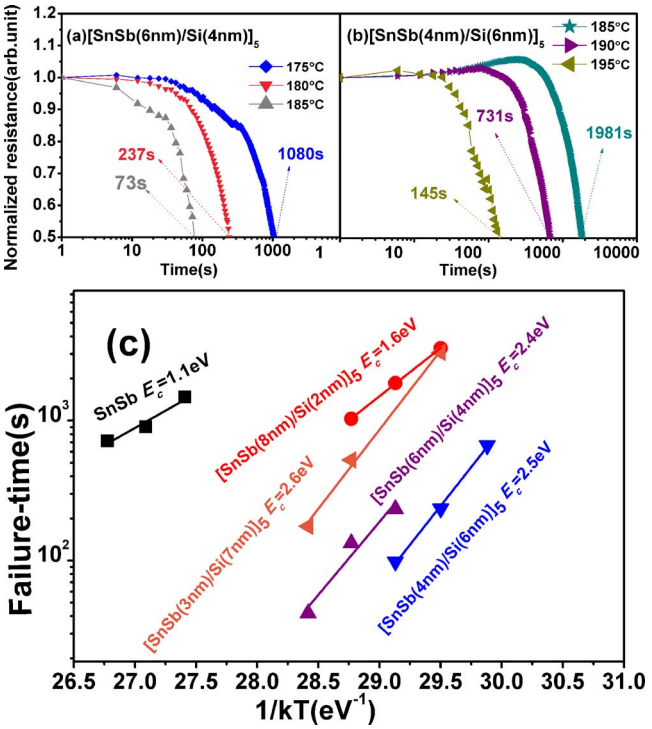

Figure 2. Normalized resistance as a function of annealing time at various temperatures for (a) $[Sn_{20}Sb_{80}(6nm)/Si(4nm)]_5$ thin film; (b) $[Sn_{20}Sb_{80}(4nm)/Si(6nm)]_5$ thin film; (c) The Kissinger plots Failure-time versus $1/kT$ of monolayer $Sn_{20}Sb_{80}$ and $Sn_{20}Sb_{80}$/Si multilayer composite thin films.

According to the Arrhenius equation:[17]

$$t = \tau_0 exp\,(E_c/k_B T) \quad [1]$$

Where t, τ_0, k_B and T represent the failure time, the constant dependent on film performance, boltzman constant and absolute temperature constant respectively. The slope of the curve in Fig. 2c represents the crystallization activation energy (E_c) of the phase-change film. Obviously, E_c of monolayer-layer $Sn_{20}Sb_{80}$ is 1.1 eV. With the increase of the relative thickness of Si layer in $Sn_{20}Sb_{80}$/Si multilayer composite films, the E_c of the composite films gradually increases ($[Sn_{20}Sb_{80}(8nm)/Si(2nm)]_5$: 1.6 eV, $[Sn_{20}Sb_{80}(6nm)/Si(4nm)]_5$: 2.4 eV, $[Sn_{20}Sb_{80}(4nm)/Si(6nm)]_5$: 2.5 eV, $[Sn_{20}Sb_{80}$ $(3nm)/Si(7nm)]_5$: 2.6 eV). It reveals that greater activation energy will increase the potential crystalline barrier of the phase change film, thus improving the thermal stability of amorphous films.

The effect of the Si alternate layers on the electrical properties of the $Sn_{20}Sb_{80}$/Si multilayer films can be studied by the bandgap. In the experiment, the reflectance spectrum of phase-change thin films was measured using a near-infrared spectrophotometer. The amorphous reflectance of the $Sn_{20}Sb_{80}$/Si multilayer films are measured, and the bandgap can be obtained by calculation and fitting. According to the formula:[18]

$$K/S = (1\text{-}R)^2/(2R) \quad [2]$$

Where R is the reflectance, K is the absorption coefficient, and S is the scattering coefficient. The intercept of energy axis is the value of bandgap. As shown in Fig. 3, the bandgap of monolayer $Sn_{20}Sb_{80}$ film is 0.357 eV. When the relative thickness of Si layer in $Sn_{20}Sb_{80}$/Si multilayer films becomes larger, the bandgap increases accordingly. Therefore, the band gaps of $[Sn_{20}Sb_{80}(8nm)/Si(2nm)]_5$, $[Sn_{20}Sb_{80}(6nm)/Si(4nm)]_5$, $[Sn_{20}Sb_{80}(4nm)/Si(6nm)]_5$ and $[Sn_{20}Sb_{80}(3nm)/Si(7nm)]_5$ multilayer films are 0.365, 0.372, 0.386 and 0.474 eV, respectively. With a broader

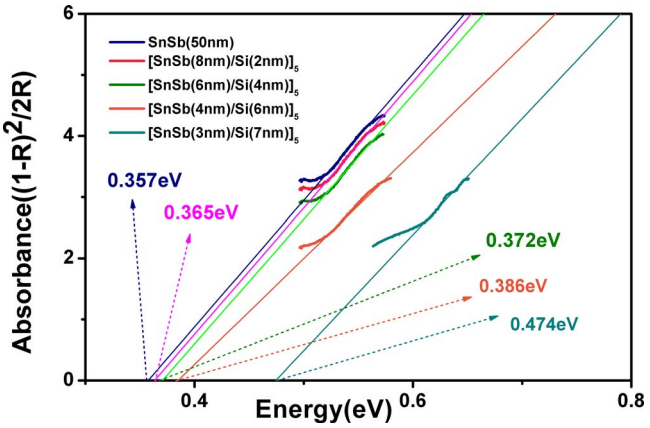

Figure 3. The Kubelka–Munk function of $Sn_{20}Sb_{80}$ and $Sn_{20}Sb_{80}$/Si thin films.

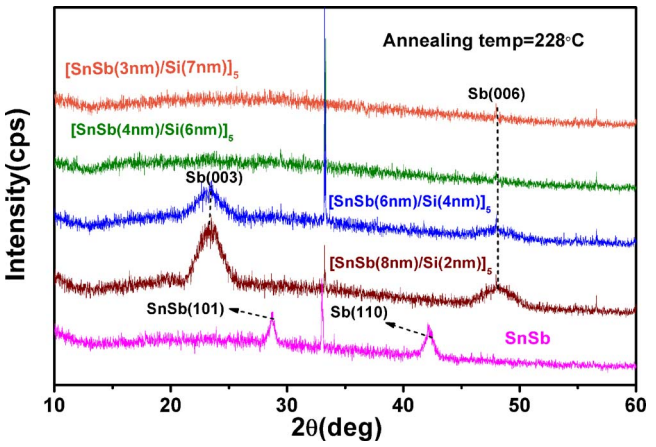

Figure 4. XRD patterns of $Sn_{20}Sb_{80}$ and $Sn_{20}Sb_{80}$/Si thin films annealed at 228°C for 30 min.

bandgap, the internal carriers have bigger energy barrier to jump from valence band to conduction band.[19] As a result, the carrier concentration will decrease and the conductivity of the films becomes worse. In $Sn_{20}Sb_{80}$/Si multilayer films, the carriers are mainly provided by $Sn_{20}Sb_{80}$. When the thickness of Si layers increases, the reflection of carriers in the interfaces will be enhanced.[20] Consequently, the resistivity will increase with thicker Si alternate layer, which is consistent with the conclusions in Fig. 1 above.

Fig. 4 shows the XRD curves of a monolayer-layer $Sn_{20}Sb_{80}$ and multilayer composite $Sn_{20}Sb_{80}$/Si thin films annealed at 228°C for 30 minutes. For the monolayer layer $Sn_{20}Sb_{80}$ film, the diffraction peaks (101) of SnSb phase and (110) of Sb phase appear after annealing. However, in $[Sn_{20}Sb_{80}(8nm)/Si(2nm)]_5$ and $[Sn_{20}Sb_{80}(6nm)/Si(4nm)]_5$, the SnSb phase disappears and the (003) and (006) diffraction peaks of the Sb phase are observed. As the thickness ratio of $Sn_{20}Sb_{80}$ in $Sn_{20}Sb_{80}$/Si decreases, the diffraction peaks of the Sb phase gradually become smaller or even disappears, indicating that the degree of crystallization is decreasing. At the same time, no diffraction peak of Si is observed, proving that Si layers exist in amorphous state. The amorphous Si alternate layers can inhibit the crystallization of $Sn_{20}Sb_{80}$ in the multi-layer films, thereby increasing the thermal stability of the composite films.[21]

The roughness of the film affects the quality and performance of the device. If the roughness of the film is too large, it may cause deterioration of device performance or device failure. Before the Atomic Force Microscope (AFM) measurement, three composite films of $[Sn_{20}Sb_{80}(8nm)/Si(2nm)]_5$, $[Sn_{20}Sb_{80}(4nm)/Si(6nm)]_5$ and $[Sn_{20}Sb_{80}(3nm)/Si(7nm)]_5$ are annealed at 320°C for 30 min. The three-dimensional shapes of the AFM are shown in Fig. 5. It can be clearly seen that $[Sn_{20}Sb_{80}(8nm)/Si(2nm)]_5$, $[Sn_{20}Sb_{80}(4nm)/Si(6nm)]_5$ and $[Sn_{20}Sb_{80}(3nm)/Si(7nm)]_5$ have the Root-Mean-Square (RMS) of 2.143, 0.817 and 0.753 nm, respectively. That is, the surface of the films becomes smoother with the increase of the thickness of Si alternate layers in $Sn_{20}Sb_{80}$/Si films. In phase switching process, the internal stress will change with the density fluctuation of phase change material.[22] The lower internal stress can ensure a good contact between the phase change film and electrode, thus improving the reliability and fatigue performance of PCM devices.

In the phase change process, the resistivity changes along with the change of reflectivity. Time-resolved pump-probe transmission spectroscopy is used to study the of the reflectivity evolution of samples. The nanosecond laser pulses are generated from a Kerr lens modelock Ti: sapphire oscillator, and have the duration of 30 ps. The laser pulses are directed into a typical pump-probe setup, and split into a pair of pulses, stronger pulse as pump and weaker pulse as probe with >15 ratio of the pump to probe in intensity. The pump and probe pulses transmit through a convex lens of 50 mm focal length and are focused to a same area on the surface of the samples. The transmitted probe after the sample is detected by a Si photodiode whose output electrical signal is sent to a lock-in amplifier so that transient

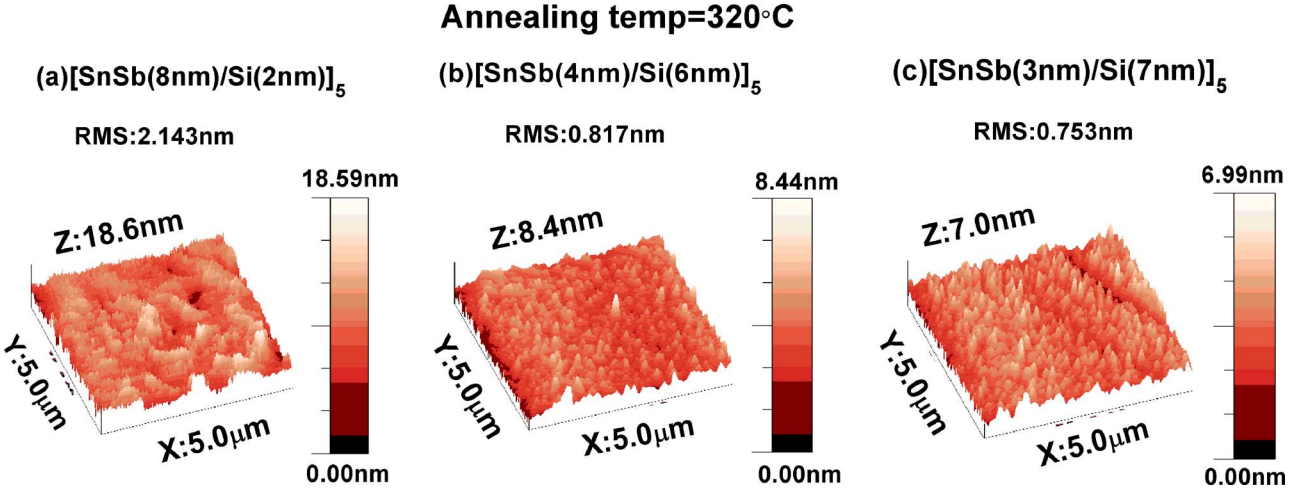

Figure 5. Three-dimensional AFM topographic images annealed 320°C for 30 min for (a) $[Sn_{20}Sb_{80}(8nm)/Si(2nm)]_5$; (b) $[Sn_{20}Sb_{80}(4nm)/Si(6nm)]_5$; (c) $[Sn_{20}Sb_{80}(3nm)/Si(7nm)]_5$.

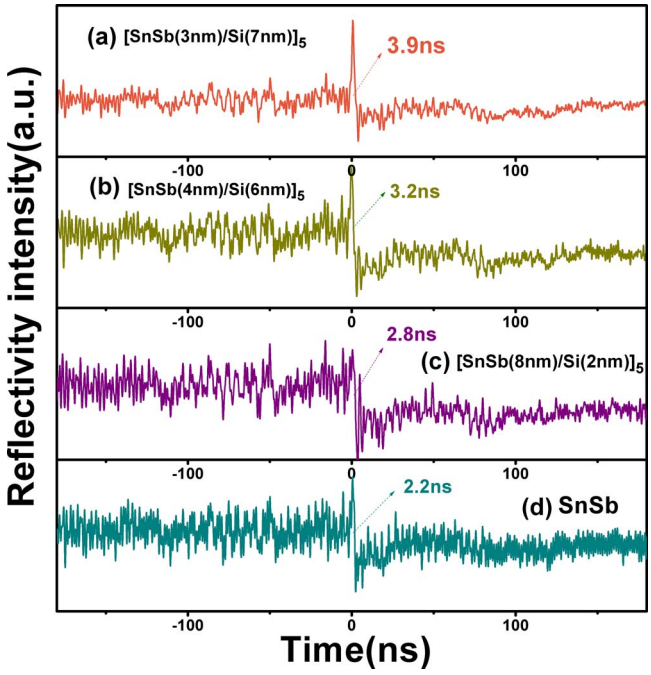

Figure 6. Reflectivity evolutions in the amorphization process for (a) $[Sn_{20}Sb_{80}(3nm)/Si(7nm)]_5$; (b) $[Sn_{20}Sb_{80}(4nm)/Si(6nm)]_5$; (c) $[Sn_{20}Sb_{80}(8nm)/Si(2nm)]_5$; (d) $Sn_{20}Sb_{80}$.

differential transmission change of the probe can be measured. Fig. 6 shows the reflectivity change of monolayer $Sn_{20}Sb_{80}$ and multilayer composite $Sn_{20}Sb_{80}$/Si thin films in the amorphization process under laser picosecond irradiation. The speed of phase change is studied using picosecond laser detection system. When a large laser pulse is applied, the reflectance of the film is significantly reduced, corresponding to the phase change from crystalline to amorphous state. The results show that the monolayer $Sn_{20}Sb_{80}$ film has the shortest switching time (2.2 ns). After compositing with Si layers, the amorphization time increase slightly with $[Sn_{20}Sb_{80}(8nm)/Si(2nm)]_5$: 2.8 ns; $[Sn_{20}Sb_{80}(4nm)/Si(6nm)]_5$: 3.2 ns; $[Sn_{20}Sb_{80}(3nm)/Si(7nm)]_5$: 3.9 ns. It manifests that the $Sn_{20}Sb_{80}$/Si multilayer thin films have a faster phase change speed than $Ge_2Sb_2Te_5$ film (17.7 ns).[23] A great deal of rich Sb phases in $Sn_{20}Sb_{80}$ layers and the lower thermal conductivity of multi-layer structure may contribute together to the ultrafast switching speed in $Sn_{20}Sb_{80}$/Si multilayer thin films.[24]

Conclusions

In summary, the phase change temperature of $Sn_{20}Sb_{80}$/Si phase change film is affected after the adding of Si alternate layers. As the thickness of the Si layer increases in the composite films, the crystallization temperature T_c of the composite films increased from 192°C of the monolayer $Sn_{20}Sb_{80}$ film to 246°C of $[Sn_{20}Sb_{80}(3nm)/Si(7nm)]_5$. The crystallization activation energy also increased from 1.1 to 2.6 eV. In addition, the amorphous $[Sn_{20}Sb_{80}(3nm)/Si(7nm)]_5$ film had a wider bandgap (0.408 eV) and a lower carrier concentration. XRD images showed that Si layer inhibited the crystallization of $Sn_{20}Sb_{80}$/Si multilayer composite films. Compared with $[Sn_{20}Sb_{80}(8nm)/Si(2nm)]_5$ and $[Sn_{20}Sb_{80}(4nm)/Si(6nm)]_5$, $[Sn_{20}Sb_{80}(3nm)/Si(7nm)]_5$ film had a smoother surface, thus ensuring reliable contact between phase change film and electrode. The $[Sn_{20}Sb_{80}(8nm)/Si(2nm)]_5$ film had a fast phase change rate of 2.8 ns. These results indicate that the $Sn_{20}Sb_{80}$/Si multilayer composite films have both faster speed and better stability for PCM applications.

Acknowledgments

This work was supported by National Natural Science Foundation of China (No. 11774438) and Natural Science Foundation of Jiangsu Province (BK20151172) and sponsored by Qing Lan Project and Postgraduate Research and Practice Innovation Program of Jiangsu Province (SJCX18_1024) and the Opening Project of State Key Laboratory of Silicon Films (SKL2017-04) and the Opening Project of Key Laboratory of Microelectronic Devices & Integrated Technology, Institute of Microelectronics, Chinese Academy of Sciences and Postgraduate Research.

ORCID

Xuan Guo https://orcid.org/0000-0003-4584-6950
Yifeng Hu https://orcid.org/0000-0001-7088-6829

References

1. X. Zhou, M. Xia, F. Rao, L. Wu, X. Li, Z. Song, S. Feng, and H. Sun, *ACS Appl. Mat. Interfaces.*, **6**, 14207 (2014).
2. M. C. Sun, B. Shen, C. Z. Wang, S. N. Song, Z. T. Song, and J. W. Zhai, *Electrochem Solid S. T.*, **15**, H115 (2012).
3. Y. F. Hu, J. W. Zhai, H. R. Zeng, S. N. Song, and Z. T. Song, *J. Appl. Phys.*, **117**, 175704 (2015).
4. X. L. Zhou, L. C. Wu, Z. T. Song, F. Rao, K. Ren, C. Peng, S. N. Song, B. Liu, L. Xu, and S. L. Feng, *Appl. Phys. Lett.*, **103**, 072114 (2013).
5. C. C. Chang, P. C. Chang, K. F. Kao, T. R. Yew, M. J. Tsai, and T. S. Chin, *IEEE. T. Magn.*, **47**, 645 (2011).
6. Z. F. He, W. H. Wu, X. Y. Liu, J. W. Zhai, T. S. Lai, S. N. Song, and Z. T. Song, *Mater. Lett.*, **185**, 399 (2016).
7. Y. F. Hu, Z. F. He, J. W. Zhai, P. Z. Wu, T. S. Lai, S. N. Song, and Z. T. Song, *Appl. Phys. A-Mater.*, **121**, 1125 (2015).
8. L. Yi, Y. F. Hu, L. Yuan, X. Q. Zhu, H. Zou, L. Shen, and Z. T. Song, *J. Non-cryst. Solids.*, **432**(Part B), 505 (2016).
9. Y. F. Hu, H. Zou, L. Yuan, J. Z. Xue, Y. X. Sui, W. H. Wu, J. H. Zhang, X. Q. Zhu, S. N. Song, and Z. T. Song, *Scripta Mater.*, **115**, 19 (2016).
10. S. Y. Chen, W. H. Wu, J. W. Zhai, S. N. Song, and Z. T. Song, *Mater. Sci. Eng. B-Adv.*, **218**, 59 (2017).
11. W. H. Wu, Y. F. Hu, X. Q. Zhu, Y. X. Sui, L. Yuan, L. Zheng, H. Zou, Y. M. Sun, S. N. Song, and Z. T. Song, *J. Mater. Sci-Mater El.*, **27**, 2183 (2016).
12. G. Ruitenberg, A. K. Petford-Long, and R. C. Doole, *J. Appl. Phys.*, **92**, 3116 (2002).
13. M. C. Sun, S. N. Song, Z. T. Song, J. W. Zhai, G. F. Liang, and Y. Q. Wu, *Scripta Mater.*, **68**, 522 (2013).
14. H. Zou, X. Q. Zhu, Y. F. Hu, Y. X. Sui, L. Zheng, W. H. Wu, L. J. Zhai, J. Z. Xue, and Z. T. Song, *J. Mater. Sci-Mater El.*, **28**, 3806 (2017).
15. Y. F. Hu, H. Zou, J. H. Zhang, J. Z. Xue, Y. X. Sui, W. H. Wu, L. Yuan, X. Q. Zhu, S. N. Song, and Z. T. Song, *Appl. Phys. Lett.*, **107**, 263105 (2015).
16. H. P. You, Y. F. Hu, X. Q. Zhu, H. Zou, S. N. Song, and Z. T. Song, *J. Mater. Sci-Mater El.*, **28**, 10199 (2017).
17. S. Sharda, N. Sharma, P. Sharma, and V. Sharma, *Mater. Chem. Phys.*, **134**, 158 (2012).
18. F. Tong, X. S. Miao, Y. Wu, Z. P. Chen, H. Tong, and X. M. Cheng, *Appl. Phys. Lett.*, **97**, 261904 (2010).
19. S. Kumar, D. Singh, S. Shandhu, and R. Thangaraj, *Appl. Surf. Sci.*, **258**, 7406 (2012).
20. X. L. Zhou, L. C. Wu, Z. T. Song, F. Rao, K. Ren, C. Peng, B. Liu, D. N. Yao, S. L. Feng, and B. M. Chen, *Thin Solid Films.*, **520**, 1155 (2011).
21. Y. F. Hu, X. Y. Feng, S. M. Li, T. S. Lai, S. N. Song, Z. T. Song, and J. W. Zhai, *Scripta Mater.*, **93**, 4 (2014).
22. H. Zou, X. Q. Zhu, Y. H. Hu, Y. X. Sui, Y. M. Sun, J. H. Zhang, L. Zheng, and Z. T. Song, *J. Appl. Phys.*, **120**, 245303 (2016).
23. Y. G. Lu, M. Wang, S. N. Song, M. J. Xia, Y. Jia, X. Shen, G. X. Wang, S. X. Dai, and Z. T. Song, *Appl. Phys. Lett.*, **109**, 17 (2016).
24. D. M. Wang, Y. G. Lu, S. N. Song, M. Wang, X. Shen, G. X. Wang, S. X. Dai, and Z. T. Song, *Acta. Phys. Sin.*, **64**, 15 (2015).